A re-appraisal of the petrogenesis and tectonic setting of the Ordovician Fishguard Volcanic Group, SW Wales

Bethan A. Phillips[1]*, *Andrew C. Kerr*[1], *Richard Bevins*[2]

1. School of Earth and Ocean Sciences, Cardiff University, Park Place, Cardiff CF10 3AT, Wales

2. Department of Natural Sciences, National Museum Cardiff, Cathays Park, Cardiff CF10 3NP, Wales

* Corresponding author

Abstract

The Fishguard Volcanic Group represents an excellently preserved example of a volcanic sequence linked to the closure of the Iapetus Ocean. This study re-examines the petrogenesis and proposed tectonic setting for the Llanvirn (467-458 Ma) Fishguard Volcanic Group, South Wales, UK. New major and trace element geochemical data and petrographic observations are used to re-evaluate the magma chamber processes, mantle melting and source region. The new data reveal that the Fishguard Volcanic Group represents a closely related series of basalts, basaltic andesites, dacites and rhyolites originating from a spinel lherzolite source which had been modified by subduction components. The rocks of the Fishguard Volcanic Group are co-genetic and the felsic members are related to the more primitive basalts mainly by low pressure fractional crystallisation. The geochemistry of the lavas was significantly influenced by subduction processes associated with a coeval arc, while significant amounts of assimilation of continental crust along with fractional crystallisation appear to have contributed to the compositions of the most evolved lavas. The Fishguard Volcanic Group was erupted into a back-arc basin where extensive rifting, but no true seafloor spreading had occurred.

Keywords: Geochemistry, Magmatism, Back-arc basin, Subduction

1. Introduction

The closure of the Iapetus Ocean (510-410 Ma) was one of the most significant events in the geological evolution of northwestern Europe (e.g., Trench & Torsvik, 1992; Cocks & Torsvik, 2006; Murphy & Nance, 2008; van Staal et al., 2009; Cocks & Torsvik, 2011). However, our understanding of the tectonomagmatic development, both of this ocean and of the marginal subduction zones along which Iapetus oceanic crust was ultimately consumed, is restricted to somewhat limited exposures. The igneous rocks of the Fishguard Volcanic Group in southwest Wales represent an excellently preserved example of rocks associated with the closure of the Iapetus Ocean.

During the emplacement of the Fishguard Volcanic Group in the early-middle Ordovician (485-458 Ma), Wales formed part of the southern margin of the closing Iapetus Ocean. Avalonia, (the microcontinent of which Wales was a part), and moved northward from 55°S to 30°S in the period from the Arenig (478-467 Ma) to the Ashgill (451-444 Ma) (Fitton et al., 1982). During this period a number of island arc chains and marginal basins formed above the south-eastward dipping subduction zone on the north side of Avalonia along a NE-SW-trending plate margin (Fitton & Hughes 1970; Phillips et al., 1976; Fitton et al., 1982; Murphy & Nance, 2008; Murphy et al., 2011). Ordovician sequences of both basic and/or silicic lavas are present not only in the Fishguard region but throughout Wales, in areas such as Snowdonia and Ramsey Island (Fig. 1) (Kokelaar et al., 1984a).

A re-evaluation of the Fishguard Volcanic Group is required as earlier studies were based on a limited range of geochemical elements. Furthermore, previous geochemical investigations have shown that the rocks are similar in composition to present-day MORB, while also displaying a relative depletion in Nb (Bevins, 1982). However, the use of tungsten carbide crushing mills in these earlier studies may have affected the Nb concentration of the rocks (e.g., Hickson & Juras, 1986) and so to avoid this problem this study has used agate

crushing mills. This study presents new major and trace element geochemical data and petrographic observations to re-evaluate the petrogenesis and tectonic setting of the Llanvirn-age (467-458 Ma) Fishguard Volcanic Group.

2. Local Geology and Previous Work

Most of the Ordovician volcanism in west Wales occurred in the period from Arenig to Llanvirn (478-458Ma) (Thomas & Thomas, 1956; Bevins & Roach, 1979). The overall consensus is that the Ordovician rocks of Wales were emplaced in a supra-subduction back-arc basin, in a mostly submarine environment on immature continental crust on the south-east side of the Iapetus Ocean (Bevins, 1982; Bevins et al., 1984; Kokelaar et al., 1984a; Leat et al., 1986). All of the Lower Palaeozoic rocks in Wales and the Welsh Borderland were affected by low-grade (zeolite to low grade greenschist facies) metamorphism, primarily due to burial (Bevins & Rowbotham, 1983; Bevins & Robinson, 1988; Robinson et al., 1999).

Early work on the geology of the area was reported by Reed (1895), Cox (1930) and Thomas & Thomas (1956). The Fishguard Volcanic Group (Reed, 1985; Thomas & Thomas, 1956; Bevins, 1979; Bevins, 1982; Bevins et al., 1984; Kokelaar et al., 1984a; Leat et al., 1986; Bevins et al., 1991) is located in the Strumble Head to Fishguard area of north Pembrokeshire, Wales (Fig. 1), close to the older Trefgarn basaltic andesite to andesite lavas of Tremadoc age (485-478Ma) which are thought to represent the products of a volcanic arc (Bevins et al., 1984).

Fishguard Volcanic Group samples were collected from an area around the Strumble Head Peninsula, (Fig. 1, Fig. 2). The volcanic group comprises three formations, from oldest to youngest: 1) the predominantly rhyodacitic to rhyolitic Porth Maen Melyn Volcanic

Formation, 2) the pillowed basalts of the Strumble Head Volcanic Formation and 3) the rhyolitic Goodwick Volcanic Formation (Bevins, 1982) (Fig. 2).

The Porth Maen Melyn Volcanic Formation (Bevins & Roach, 1979) is composed principally of rhyolitic tuffs, ash flow tuffs, rhyolite lavas, autobreccias, debris flow breccias and, to a lesser extent, massive and pillowed rhyodacite lavas. Small volumes of intermediate magmas were also emplaced as microtonalite intrusions (Bevins & Roach, 1979).

Conformably overlying this formation is the Strumble Head Volcanic Formation. Basaltic pillow lavas with well-developed inter-pillow breccias, local elongate steeply inclined lava tubes and necking structures are found at the contact with the Porth Maen Melyn Volcanic Formation (Bevins, 1982). The formation also comprises massive lensoid lava sheets, thin hyaloclastites, basaltic Tuffs, rare rhyolitic tuff horizons and high-level intrusive basaltic sheets (Bevins & Roach, 1979). The boundary between this formation and the overlying rhyolitic Goodwick Volcanic Formation is marked by a complex interdigitation of lavas and high-level intrusions (Kokelaar et al., 1984b).

The Goodwick Volcanic Formation progresses stratigraphically upwards through thick rhyolitic domes and flows to autobrecciated rhyolites and fine tuffaceous silicic rocks which are intruded by a thick basic sill. The sill is bulbous at the base and pillowed at the top indicative of having been intruded into wet sediment (Kokelaar et al., 1984b).

The volcanic group is composed of up to 1.8 km of volcanic and intrusive rocks, deposited in locally subsiding basin (Kokelaar et al., 1984a; Kokelaar et al., 1984b). The rocks were extruded in a mostly submarine environment with restricted occurrences of subaerial volcanism (Bevins, 1982; Kokelaar et al., 1984a; Kokelaar et al., 1984b; Kokelaar 1988). Sediment gravity flow deposits are found interstratified with the pillow lavas, although

these are not derived from the lavas and so no topographic highs are thought to have developed (Kokelaar et al., 1984a; Kokelaar et al., 1984b; Kokelaar 1988).

The basaltic and intermediate lavas and intrusions were recognised as tholeiitic by Bevins (1982) and were proposed to be derived by low-pressure fractional crystallisation of a parental magma, which originated in the upper mantle. Bevins et al. (1991) noted that some of the silicic intrusive and extrusive rocks display a calc-alkaline trend as opposed to a tholeiitic trend. It is uncertain whether dacitic and rhyolite magmas were derived from the same source as the basaltic rocks, although limited trace element data for the rhyolites reported by Bevins et al. (1991) are consistent with such an origin.

3. Petrography

Eighteen basic, intermediate and silicic rocks from the samples collected by Bevins (1979) were re-examined petrographically (Supplementary Material 1). Basalt sample SB34 is from a pillow lava and contains tabular clinopyroxene, minor plagioclase, secondary chlorite and pumpellyite. Other pillowed basalts (samples SB31 and SB58) contain zoned clinopyroxene and plagioclase as microphenocrysts in a groundmass of spherulitic (quenched) clinopyroxene and plagioclase. Sample SB33 consists of tabular plagioclase and interstitial clinopyroxene with secondary chlorite and comes from a massive basaltic lava. The basaltic intrusions (samples LG3, LG1 and LG5) contain euhedral, subophitic clinopyroxene, altered tabular plagioclase, abundant chlorite and, in the case of LG5, epidote. Other intrusive basaltic sheets (samples REB166, SB22, SB44, SB28 and SB59) contain albitised plagioclase with subophitic clinopyroxene and chlorite. Samples SB54 and SB55 are also from intrusive basaltic sheets; however they comprise clinopyroxene and plagioclase phenocrysts set in a finer feldspathic groundmass along with Fe-Ti oxides. The rhyolitic flow samples (SA11 and

SA5) are fine grained with quartz-feldspar groundmass (most likely recrystallized from glass) and also contain quartz and epidote veins. Both the rhyodacite lava (sample REB94) and the microtonalite intrusion (sample REB342) contain plagioclase, quartz, chlorite and rare biotite. The field relations of these samples are discussed in detail in Bevins (1982).

4. Analytical techniques

Eighteen samples (2 rhyolites, 2 dacites and 14 basalts) from the original sample set described and collected by Bevins (1979) from a transect through the Fishguard Volcanic Group (Fig 2 and Supplementary Material 1) were re-prepared and re-analysed for major and trace elements.

Following removal of weathered surfaces, the samples were crushed in a steel jaw crusher and powdered using an agate Tema mill at Cardiff University. Major and trace element abundances were analysed using a JY Horiba Ultima 2 inductively coupled plasma optical emission spectrometer (ICP-OES) and a Thermo X7 series inductively coupled plasma mass spectrometer (ICP-MS) at Cardiff University, Wales. Further information regarding methods and instruments are discussed in McDonald & Viljoen (2006).

Accuracy and precision of the data were assessed using the international reference materials NIM-G and JB-1A (Supplementary Material 2). Relative standard deviations show accuracy of 1-5% for most major and trace elements for the standard materials used. Duplicate standard deviations are also within error, ensuring precision. A representative data set can be found in Table 1 and the full data set in Supplementary Material 3.

5. Geochemical Results

157 **5.a. Element Mobility**

158 The rocks analysed in this study have all undergone low-grade sub-greenschist facies
159 metamorphism (Bevins & Rowbotham, 1983; Robinson & Bevins, 1986) and this is reflected
160 in the abundance of chlorite observed in the thin sections along with less common
161 pumpellyite, prehnite and epidote. Varying degrees of albitization have affected the rocks and
162 so the concentrations of Al, Ca and Na in particular have been modified (Bevins 1982).
163 Under such metamorphic conditions many elements, in particular the large-ion lithophile
164 elements, become mobile. Accordingly, these elements are not representative of the original
165 magmatic composition of the rocks and so cannot be used to assess the petrogenetic processes
166 that the magmas have undergone. In this study therefore we will use trace elements generally
167 regarded to be relatively immobile during low-grade metamorphism, i.e., HFSE (High Field
168 Strength Elements) and REE (Rare Earth Elements) (e.g., Pearce & Cann, 1973; Wood et al.,
169 1979; Merriman et al., 1986).

170

171 **5. b. Classification**

172 A range of rock types is evident in the samples analysed, including basalts, basaltic
173 andesites, dacites and rhyolites (Figs. 3a - c). In Figure 3a the basalts and dacites (with the
174 exception of SB33) predominantly classify as tholeiitic, while the rhyolites are more calc-
175 alkaline. However, silica contents are susceptible to mobility during sub-solidus
176 hydrothermal alteration, and so several classification diagrams which are based on relatively
177 immobile elements have also been used, i.e., the Nb/Y vs. Zr/Ti and Co vs. Th diagrams
178 (Figs. 3b, 3c).

In Figure 3b the samples all plot in the subalkaline field as a continuum from basalt to rhyolite, and on this diagram two of the samples (SB59 and SB58) classify as basaltic andesite. On the Co-Th diagram (Fig. 3c) the majority of the samples plot in the calc-alkaline field, with four of the basalts falling in the island arc tholeiite field. While the majority of basalts plot close to the dividing line between basalt and basaltic andesite only sample SB55 plots in the basaltic andesite field. The rhyolites plot in the dacite/ rhyolite field while the dacites, fall on the andesite side of the boundary between andesite and dacite. The most evolved basalts appear to be samples SB59 and SB55, although the classification diagrams are generally inconclusive in this regard. Overall, the basalts and dacites of the group show a tholeiitic to tholeiitic/calc-alkaline transitional trend while the rhyolites have a more calc-alkaline type chemistry.

5.c. Basalt Geochemistry

The basalts show an overall trend of increasing SiO_2 with decreasing MgO and increasing TiO_2, K_2O, CaO and Fe_2O_3 with MgO. Al_2O_3 wt.% generally behaves erratically showing no correlation with MgO wt.%. Two trends are observed in the TiO_2, CaO and Fe_2O_3 vs. MgO plots (Fig. 4), one at lower MgO wt.% with a steep increase in the other major elements and the other which shows less variation in the other oxides with increasing MgO wt. %. Sample REB166 is the most primitive basalt in the suite, with a MgO of 10.8 wt. %, SiO_2 of 46.4 wt.% and Fe_2O_3 of 1.0 wt.%.

In Figure 5 selected trace elements are plotted against Zr. When immobile elements are plotted against Zr (itself immobile and incompatible in the basalts), a good correlation within the basalts indicates that the sequence of rocks are possibly co-genetic (Cann, 1970; Hastie et al., 2008). Many of the more immobile elements show a broad positive linear

correlation with Zr, (e.g., La), whereas Sc decreases as the lavas become more evolved (Fig. 5). These features suggest that the basalts may be derived from parent magmas which have been derived through similar melting conditions from a similar source.

The La/Yb ratios of the basalts range from 1.9 to 3.3. The basaltic samples generally have flat to slightly LREE-enriched chondrite-normalised REE patterns with a slight depletion in the HREE (Fig. 6a). The basalts are somewhat enriched compared to N-MORB, particularly for the more incompatible elements on the left hand-side of the N-MORB-normalised plot and generally have variable negative Nb anomalies, except sample REB166 (Fig. 6b). As the basalts become more evolved so they become more enriched in incompatible trace elements and develop a progressively more marked negative Eu anomaly (Figs. 5e, 6b).

5.d. Dacite and Rhyolite Geochemistry

The evolved samples contain more Si and K along with less Ti, Ca and Fe than the basaltic rocks. The major element compositions variations range from e.g. 64.7 – 76.1 wt.% SiO_2 and from1.3 – 6.3 wt.% K_2O in a linear array (Fig. 4). The trace element variations vs. Zr (Fig. 5) for the more evolved samples are more scattered than for the basalts, although, a broad linear trend is observed for La and Nb (Figs. 5a, 5d). The Zr content increases from the basalts to the dacites before falling again in the rhyolites which may indicate Zr saturation followed by fractionation. The lack of coherent trace element trends both between the basalts and the evolved rocks, and within the evolved rocks themselves is most likely a reflection of Zr's incompatibility in the basalts and dacites and compatibility in the rhyolites. This is especially evident from the Th-Zr variation diagram, which shows a co-genetic trend for the basalts, while the data for the rhyolites and dacites are more scattered (Fig. 5b).

226 The La/Yb ratio of the dacites varies from 3.8 - 7.3, while the rhyolites vary from 4.6
227 – 6.1. The rhyolites and dacites are significantly more enriched in the LREE [$(La/Sm)_{CN}$ >3]
228 (chondrite normalised; Sun and McDonough, 1989) than the basalts [$(La/Sm)_{CN}$ <3] but have
229 similar, relatively flat, HREE patterns (Figs. 6a - b). All of the dacites and rhyolites possess
230 negative Nb anomalies (Fig. 6b). The more evolved rocks also show more marked negative
231 Eu anomalies than the basalts indicating separation of plagioclase during low pressure crystal
232 fractionation from a more basic magma (Figs. 5e, 6a).

233

234 **6. Discussion**

235

236 **6.a. Mantle source composition**

237 Modern day back-arc basins are underlain by both oceanic and continental crust
238 formed by either seafloor spreading, rifting of older arc or continental crust (Sinton et al.,
239 2003; Martinez et al., 2006). However, the relative proportions of these types of crust are
240 often a matter of considerable debate, (Stern, 2002). The formation of oceanic crust in back-
241 arc basins is thought to be mainly controlled by two different melt generation processes;
242 hydrous flux melting (e.g., Tatsumi & Eggins, 1995) and decompression melting during
243 seafloor spreading (e.g., Langmuir et al., 1992). With increasing distance of the back arc
244 spreading centre from the subduction zone decompression melting tends to dominate over
245 subduction flux melting (e.g., Gribble et al., 1998; Sinton et al., 2003).

246 Factors contributing to the geochemical heterogeneity of back-arc basin basalts
247 include variations in the underlying mantle in terms of its fertility, composition and degree of
248 partial melting, lithospheric thickness, and amount of water present in the system (Pearce &

249 Stern, 2006). Variations in the subduction input, such as the nature and composition of the
250 subducted materials, will also influence the geochemistry of lava erupted in the back-arc
251 region. The melting, assimilation and crystallisation history of the lavas will also contribute
252 to the compositional diversity observed in back-arc basins. The influence of subduction zone
253 fluids should be greatest during the early stages of basin opening and then diminish as the
254 basin widens, although this is dependent on the geometry of the basin (Sinton et al., 2003;
255 Martinez et al., 2006).

256 The magmas represented by the basalts of the Fishguard Volcanic Group were most
257 likely derived from a shallow, relatively garnet-free, source (spinel lherzolite) as indicated by
258 the flat HREE patterns. This is most likely reflective of the E-W extension of immature
259 continental crust that occurred from the Tremadoc – Caradoc (485-448Ma), resulting in
260 locally subsiding grabens controlled by crustal discontinuities (Kokelaar, 1988).

261 More insights from the REE data for the rocks and so their source can be gained
262 through the use of a Dy/Dy* - Dy/Yb plot (Fig. 7a). Dy/Dy* (Dy/Dy* = $DyN/(La_N^{4/13}$
263 $Yb_N^{9/13}$) is a measure of the concavity of a REE pattern (Davidson et al., 2013) and, in
264 addition to helping determine source components, this diagram can help elucidate if
265 amphibole has been significantly involved in the petrogenesis of a magma (either by
266 fractionation or by being residual in the source). Figure 7a shows that the Fishguard lavas and
267 intrusions plot mostly in the MORB field of the diagram and display a general trend of
268 increasing Dy/Dy* with Dy/Yb. Only samples SB59 and SB54 trend towards the amphibole
269 vector, indicating minimal involvement.

270 The Th/La-$(Ce/Ce^*)_{Nd}$ diagram (Fig. 7b) which is used to determine the affinity of
271 sedimentary slab components that have contaminated the source region of subduction zone
272 rocks. The majority of the basalts plot in an array between N-MORB and the volcanic detritus

field, with some of the more evolved basalts plotting within the continental detritus field, indicating a variable subduction component within the basalts. This suggests relative proximity to the continental subduction zone.

All except one of the samples analysed in this study (REB166) are displaced above the MORB-OIB array towards the continental arc region of the Th/Yb – Nb/Yb plot (Fig. 7c) further implying proximity to a subduction zone. The subducting slab does not retain Th and therefore an increase in its concentration in the mantle wedge, and so in back-arc basin magmas, is indicative of input from a subduction zone (Pearce, 2008). An increase in the Th/Yb ratio therefore implies an increasing subduction input, while an increase in the Nb/Yb ratio is more indicative of increasing depth of melting. It is clear that the Fishguard rocks show a variable subduction influence in the basalts with little change in melting depth, in agreement with Figure 7b. Figures 7b and c suggest that sample REB166 contains a minimal amount of subduction component. The sample, highlighted in Figure 6, also shows no Nb depletion or significant Th enrichment seen in the other samples. Typically back-arc basin basalts can contain variable amounts of subduction components (Pearce et al., 2005; Pearce & Stern, 2006). In the case of the Fishguard Volcanic Group the majority of the basalts contain a substantial subduction component. These components are derived during subduction by the release of fluids and/or sediments from the slab or may have been via inherited subduction components in the lithosphere, highlighting the complexity of the source.

6. a. Crustal Processes

Bevins (1982) suggested that the various dacites, rhyodacites and rhyolites exposed in the Porth Maen Melyn and Fishguard area were derived by crystal fractionation from the

297 basic magmas. The relative roles of fractional crystallisation from basalt and generation by
298 crustal melting for the silicic rocks of the Ordivician marginal basins of Wales have been
299 debated by many authors (Kokelaar et al., 1984a; Leat et al., 1986; Thorpe et al., 1993)

300 In order to test these different models both fractional crystallisation and assimilation
301 with fractional crystallisation (AFC) modelling were carried out. Rayleigh fractional
302 crystallisation modelling was undertaken using sample LG3 as a possible parental magma as
303 it has relatively high MgO (9.1 wt. %) and also has low LREE contents. Those models were
304 calculated using PELE, a PC platform version of the silicate liquid crystallization MELTS
305 software program (Boudreau, 1999). The major element geochemical trends were modelled at
306 different pressures and water content parameters, using a quartz – fayalite – magnetite (QFM)
307 oxygen buffer to define oxygen fugacity (fO_2). The modelling at 1kbar predicts initial
308 crystallization of olivine and spinel, until ~12% crystallisation at which point plagioclase
309 begins to crystallise followed by clinopyroxene at ~39% crystallisation. This sequence is
310 generally consistent with that observed in the thin sections. Most of the samples show ophitic
311 clinopyroxene plagioclase relationships with some of the clinopyroxene also containing
312 rounded pseudomorphs of what was previously olivine. The chemistry of this mineral
313 assemblage predicted by PELE was then modelled at 10% fractionation intervals using the
314 relevant distribution coefficients (Rollinson, 1993).

315 The results presented in Figure 8 are of the models which best predict the major
316 geochemical trends observed in the data i.e., low pressure fractional crystallisation (1kbar) in
317 a magma which was either anhydrous or contained 1% H_2O. The basalt trend is more
318 accurately modelled than the dacite/ rhyolite data. The models can generally predict the SiO_2
319 and K_2O trends of the basalts and some of the more evolved rocks but cannot replicate the
320 highest values. The models predict the low CaO trend of the basalts but have higher CaO than
321 the dacites and rhyolites. The high CaO trend is most likely a result of alteration (Bevins,

1982). The FeO trend, however, is poorly replicated by the models. A low-pressure magma chamber model is in accordance with previous studies (Bevins et al., 1991) but neither fractional crystallisation model conclusively fits the observed data.

AFC modelling (DePaolo, 1981) was carried out for trace elements at 1kbar (Fig. 9). A significant limitation to the model is that Zr is incompatible in all instances, whereas in reality it is compatible in the more evolved rocks, meaning that their compositions are not reproduced in the models. Another limitation to the AFC models is that the exact nature of any potential contaminant is not known. An average composition for felsic continental crust has been used (from Rudnick & Gao, 2003) which represents a potential fusible crustal contaminant.

Marked enrichments in incompatible elements (particularly Yb, Tb, Y) observed in rhyolites and dacites (Figs. 9a, 9c, 9d) can be replicated by AFC modelling especially with higher crustal assimilation. The models cannot however replicate the elevated Th, Yb, Tb and Y concentrations of the basalts nor does any one single curve match the trend shown by the rest of the samples (Fig. 9b). These models do, however, suggest a shift from initial fractional crystallisation in the most primitive basalts to assimilation fractional crystallization in the more evolved basalts.

6.c. Tectonic Reconstruction

The evidence discussed in the previous section suggests that the rocks in this study: a) have been subjected to the influence of subduction zone components; b) have undergone some crustal contamination; and c) the basalts have a source that is compositionally similar to MORB, as evidenced by Figure 7a.

345 The mantle source composition for the primitive magmas of the Fishguard Volcanic
346 Group has been determined to be a mixture of MORB like-source mantle and subducted
347 sediment. Flat HREE patterns indicate melting took place in the spinel stability field at
348 shallow depths (<60km) and so along with the above indicate contamination of a spinel
349 lherzolite source with subduction components. Contamination of the source by continental
350 volcanic detritus (Fig. 7b) signifies an arc-proximal setting close to a continental margin
351 (e.g., Sinton et al., 2003; Martinez et al., 2006). In addition to this, the presence of spatially
352 and temporally close acidic and intermediate rocks and the lack of formation of true oceanic
353 crust (Kokelaar et al., 1984a) indicate proximity to a volcanic arc. The immature continental
354 crust on which the Fishguard basin formed (Kokelaar et al., 1984a) may have been part of a
355 rifted arc system, which originated from earlier arc volcanism in the Tremadoc represented
356 by the Trefgarn Volcanic Group (Kokelaar et al., 1984b).

357 The suite of investigated rocks shows a compositional range through basalts, basaltic
358 andesites, dacites and rhyolites. The rocks in this suite of lavas and intrusions are most likely
359 compositionally similar magmas, with any scatter likely due to variable subduction inputs,
360 fractional crystallisation and AFC. Fractional crystallisation at 1kbar can explain many of the
361 trends observed in the data. Low-pressure fractional crystallisation also generally agrees with
362 the estimated source depth and with previous studies such as Bevins et al. (1991). There may
363 have also been a hydrous component in the form of fluids or hydrous minerals (Fig. 8)
364 present during fractional crystallisation, which is consistent with a subduction zone setting
365 (Stern, 2002). AFC modelling indicates that crustal contamination also played a significant
366 role in the formation of the more evolved rocks. Furthermore, crustal contamination
367 reinforces the interpretation that the basin was formed on rifted volcanic arc crust (Kokelaar
368 et al., 1984a; Martinez et al., 2006).

The Fishguard Volcanic Group is therefore likely to have formed in a back-arc basin setting in which a compositionally continuous and genetically linked suite of lavas were erupted. It is suggested that the Fishguard Volcanic Group formed in a back-arc basin where extensive rifting but no true spreading (and oceanic crust generation) had yet occurred.

6.c.1 Regional Implications

Other Ordovician lavas erupted in the Welsh marginal basin show geochemical similarities to the Fishguard Volcanic Group. The Ramsey Island rhyolites (Middle Arenig) (Kokelaar et al., 1984a) in particular are markedly compositionally similar to the Fishguard Volcanic Group (e.g., Figs. 7b - c), which may be a reflection of their spatial and temporal proximity (Bevins et al., 1991). The rocks of the Snowdon Volcanic Group, North Wales (Fig.1) (Arenig – early Caradog) (Kokelaar et al., 1984a) are enriched in incompatible elements (Fig. 7c) with moderate to marked Fe enrichments and are transitional between tholeiitic and calc-alkaline in composition (Kokelaar et al., 1984a). Figure 7c shows that the rocks from the Snowdon Volcanic Group also contain generally higher Th/Yb ratios highlighting the more pronounced influence of subduction due to their closer proximity to the volcanic arc (e.g. Sinton et al., 2003). This may be a reflection of the control of crustal discontinuities (steep fractures at shallow levels of considerable length that have undergone repeated tectonic activity) on the volcanic location and development (Kokelaar, 1988). The Fishguard Volcanic Group by comparison shows marked Fe enrichment (Kokelaar et al., 1984a) and a tholeiitic to tholeiitic – calc alkaline transitional trend.

Figure 10 illustrates the proposed tectonic model for the origin and evolution of the Fishguard Volcanic Group. The proposed model is that the Fishguard Volcanic Group formed in a back-arc basin in which rifting and extension of immature continental crust (which may

represent rifted arc crust) had occurred. The locus of extension most likely occurred between the active and rifted arc, where the system is rheologically weakest (Sdrolias and Müller, 2006). The magmas originated partially from flux melting in the mantle wedge, with this melting facilitated by fluids expelled from subducting slab sediments. Decompression melting at relatively shallow depths, associated with the rifting of the basin also took place. The magmas underwent fractional crystallisation, during which crustal contamination from the immature continental crust of the rifted arc took place.

There are several other known Ordovician Avalonian terranes that have comparable magmatism and originated in similar tectonic settings to the Welsh marginal basin rocks. Similar terranes from the southern flank of the Iapetus include the Antigonish Highlands Avalonian terrane in Nova Scotia, Canada and the Avoca volcanic rocks, Ireland; both formed due to rifting within an overall arc environment (McConnell et al., 1991; Murphy et al., 2011). These comparable origins therefore reinforce the suggested model of formation for the Fishguard Volcanic Group.

7. Conclusions

1. The Fishguard Volcanic Group formed in a back-arc basin in close proximity to a subduction zone.
2. Geochemical evidence and modelling indicates a shallow (garnet-free) lherzolite source for the Fishguard Volcanic Group. Subduction inputs and low-pressure (1kbar) fractional crystallisation are the more influential processes in the petrogenesis of the basalts, while crustal contamination was a significant processes in the formation of the more evolved rocks of the Fishguard Volcanic Group.

3. The immature continental crust nature of the basin may be derived from a rifted arc crust (Kokelaar et al., 1984a) which coupled with the suggested shallow source region, indicates that previous extension had occurred in the basin. This is consistent with the evidence for earlier volcanic arc activity in this region during the Tremadoc (485-478Ma) (Kokelaar et al., 1984a).
4. It is therefore suggested that the Fishguard Volcanic Group was generated in a back-arc basin setting where extensive rifting (but no seafloor spreading) has occurred (Fig. 10).

8. Acknowledgements

This study forms part of the first author's MESci Thesis completed at Cardiff University. Iain McDonald is thanked for the major and trace element analyses of the samples. We also thank Jake Ciborowski for beneficial geochemical discussions. This manuscript benefited greatly from reviews by Brendan Murphy and Mike Fowler and editorial comments by Phil Leat.

9. References

BEVINS, R .E. 1979. The geology of the Strumble Head-Fishguard region, Dyfed, Wales. Unpublished Ph.D. thesis, University of Keele, 256 pages.

BEVINS, R .E. 1982. Petrology and geochemistry of the Fishguard Volcanic Complex, Wales. *Geological Journal*, **17**, 1-21

438 BEVINS, R. E. & ROACH, R. A. 1979. Early Ordovician volcanism in Dyfed, SW Wales. In
439 *The Caledonides of the British Isles – Reviewed*, (eds Harris, A.L., Holland, C.H. and
440 Leake, B.E), Geological Society of London Special Publication, **8,** 603–9
441
442 BEVINS, R. E. & ROWBOTHAM, G. 1983. Low grade metamorphism within the Welsh
443 sector of the paratectonic Caledonides. *Geological Journal,* **18**, 141-168
444
445 BEVINS, R. E., KOKELAAR, B. P. & DUNKLEY, P. N. 1984. Petrology and geochemistry of
446 lower to middle Ordovician igneous rocks in Wales: a volcanic arc to marginal basin
447 transition. *Proceedings of the Geologists' Association*, **95**, 337-347
448
449 BEVINS, R. E. & ROBINSON, D. 1988. Short Paper: Low grade metamorphism of the Welsh
450 Basin Lower Palaeozoic succession: an example of diastathermal
451 metamorphism? *Journal of the Geological Society*, **145**, 363-366
452
453 BEVINS, R. E., LEES, G. J. & ROACH, R. A. 1991. Ordovician bimodal volcanism in SW
454 Wales: geochemical evidence for petrogenesis of the silicic rocks. *Journal of the*
455 *Geological Society*, **148**, 719-729
456
457 BOUDREAU, A. 1999. PELE---a version of the MELTS software program for the PC
458 platform. *Computers and Geosciences*, **25**, 201-203
459
460 CANN, J. R. 1970. Rb, Sr, Y, Zr and Nb in some ocean floor basaltic rocks. *Earth and*
461 *Planetary Science Letters*, **10**, 7-11
462

463 COCKS, L. R. M., & TORSVIK, T. H. 2006. European geography in a global context from
464 the Vendian to the end of the Palaeozoic. *Memoirs-Geological Society of London*, **32**, 83
465
466 COCKS, L. R. M., & TORSVIK, T. H. 2011. The Palaeozoic geography of Laurentia and
467 western Laurussia: a stable craton with mobile margins. *Earth-Science Reviews*, **106**, 1-
468 51.
469
470 COX, A. H. 1930. Preliminary note on the geological structure of Pen Caer and Strumble
471 Head, Pembrokeshire. *Proceedings of the Geologists' Association*, **41**, 274–89
472
473 DAVIDSON, J., TURNER, S. & PLANK, T. 2013. Dy/Dy*: Variations arising from mantle
474 sources and petrogenetic processes. *Journal of Petrology*, **54**, 525-537
475
476 DEPAOLO, D. J. 1981. Trace element and isotopic effects of combined wallrock
477 assimilation and fractional crystallization. *Earth and Planetary Science Letters*, **53**, 189-
478 202
479
480 FITTON J. G. & HUGHES D. J. 1970. Volcanism and plate tectonics in the British
481 Ordovician. *Earth and Planetary Science Letters*, **8**, 223–228
482
483 FITTON, J. G., THIRLWALL, M. F. & HUGHES, D. J. 1982. Volcanism in the Caledonian
484 orogenic belt of Britain. In *Andesites*, (eds Thorpe, R. S.) 611-36. Wiley, London.
485

GRIBBLE, R.F., STERN, R.J., NEWMAN, S., BLOMMER, S.H. & O'HEARN. T. 1998. Chemical and isotopic composition of lavas from the northern Mariana Trough: Implications for magma genesis in back-arc basin. *Journal of Petrology,* **39**, 125–154

HASTIE, A. R., KERR, A. C., PEARCE, J. A. & MITCHELL, S. F. 2007. Classification of altered volcanic island arc rocks using immobile trace elements: development of the Th–Co discrimination diagram. *Journal of Petrology*, **48**, 2341-2357

HASTIE, A. R., KERR, A. C., MITCHELL, S. F. & MILLAR, I. L. 2008. Geochemistry and petrogenesis of Cretaceous oceanic plateau lavas in eastern Jamaica. *Lithos*, **101**, 323-343

HASTIE, A. R., MITCHELL, S. F., TRELOAR, P. J., KERR, A. C., NEILL, I. & BARFOD, D. N. 2013. Geochemical components in a Cretaceous island arc: The Th/La–$(Ce/Ce^*)_{Nd}$ diagram and implications for subduction initiation in the inter-American region. *Lithos*, **162–163**, 57-6

HICKSON, C. J., & JURAS, S. J. 1986. Sample contamination by grinding. *Canadian Mineralogist*, **24** (3), 585-9

KOKELAAR, B. P. 1988. Tectonic controls of Ordovician arc and marginal basin volcanism in Wales. *Journal of the Geological Society*, **145** (5), 759-775.

KOKELAAR, B. P., HOWELLS, M. F., BEVINS, R. E., ROACH, R. A. & DUNKLEY, P. N. 1984a. The Ordovician marginal basin in Wales. In *Volcanic and Associated Sedimentary*

and Tectonic Processes in Modern and Ancient Marginal Basins (eds Kokelaar, B.P & Howells, M.F), Geological Society Special Publication, **16**, 245–69

KOKELAAR, B. P., HOWELLS, M. F., BEVINS, R. E. & ROACH, R. A. 1984b. Volcanic and associated sedimentary and tectonic processes in the Ordovician marginal basin of Wales: a field guide. In *Volcanic and Associated sedimentary and Tectonic Processes in Modern and Ancient Marginal Basins* (eds. Kokelaar, B.P & Howells, M.F), Geological Society Special Publication, **16**, 291–322

LANGMUIR, C. H., KLEIN, E. M. & PLANK. T. 1992. Petrological systematics of mid-ocean ridge basalts: Constraints on melt generation beneath ocean ridges. In *Mantle Flow and Melt Generation at Mid-Ocean Ridges*. (eds Phipps Morgan, J., Blackman, D.K. & Sinton, J.M), American Geophysical Union, Washington, DC. 183–280

LEAT, P. T., JACKSON, S. E., THORPE, R. S. & STILLMAN, C. J. 1986. Geochemistry of bimodal basalt-subalkaline/peralkaline rhyolite provinces within the Southern British Caledonides. *Journal of the Geological Society*, **143**, 259-273

MARTINEZ, F., TAYLOR, B., BAKER, E. T., RESING, J. A. & WALKER, S. L. 2006. Opposing trends in crustal thickness and spreading rate along the back-arc Eastern Lau Spreading Center: Implications for controls on ridge morphology, faulting, and hydrothermal activity. *Earth and Planetary Science Letters*, **245**, 655-672

533 MCCONNELL, B. J., STILLMAN, C. J., & HERTOGEN, J. 1991. An Ordovician basalt to
534 peralkaline rhyolite fractionation series from Avoca, Ireland. *Journal of the Geological*
535 *Society*, **148**, 711-718
536
537 MCDONALD, I., & VILJOEN, K. S. 2006. Platinum-group element geochemistry of mantle
538 eclogites: a reconnaissance study of xenoliths from the Orapa kimberlite, Botswana.
539 *Applied Earth Science: Transactions of the Institutions of Mining and Metallurgy:*
540 *Section B*, **115**, 81-93
541
542 MERRIMAN, R. J., BEVINS, R. E. & BALL, T. K. 1986. Petrological and geochemical
543 variations within the Tal y Fan intrusion: a study of element mobility during low-grade
544 metamorphism with implications for petrotectonic modelling. *Journal of Petrology*, **27**,
545 1409-1436
546
547 MIYASHIRO, A. 1975. Volcanic rock series and tectonic setting. *Annual Review of Earth*
548 *and Planetary Sciences*, **3**, 251
549
550 MURPHY, J. B., & NANCE, R. D. 2008. The Pangea conundrum. *Geology*, **36**, 703-706
551
552 MURPHY, J. B., HAMILTON, M. A., & LEBLANC, B. 2011. Tectonic significance of Late
553 Ordovician silicic magmatism, Avalon terrane, northern Antigonish Highlands, Nova
554 Scotia. CJES Special Issue: In honour of Ward Neale on the theme of Appalachian and
555 Grenvillian geology. Contribution to International Geological Correlation Programme
556 (IGCP) Project 497. *Canadian Journal of Earth Sciences*, **49,** 346-358
557

PEARCE, J. A. & CANN, J. R. 1973. Tectonic setting of basic volcanic rocks determined using trace element analyses. *Earth and Planetary Science Letters*, **19**, 290-300

PEARCE, J. A., STERN, R. J., BLOOMER, S. H. & FRYER, P. 2005. Geochemical mapping of the Mariana arc-basin system: Implications for the nature and distribution of subduction components. *Geochemistry, Geophysics, Geosystems*, **6**, 2004GC000895

PEARCE, J. A. & STERN, R. J. 2006. Origin of back-arc basin magmas: trace element and isotope perspectives, in Back- Arc Spreading Systems: Geological, Biological, Chemical, and Physical. *Back-Arc Spreading Systems: Geological, Biological, Chemical, and Physical Interactions*, (eds Christie, D.M., Fisher, C. R., Lee, S.M., and Givens, S.), American Geophysical Union, Washington, D. C. 63 – 86, doi: 10.1029/166GM06

PEARCE, J. A. 2008. Geochemical fingerprinting of oceanic basalts with applications to ophiolite classification and the search for Archean oceanic crust. *Lithos*. 14-48

PHILLIPS, W. E., STILLMAN, C. J. & MURPHY T. 1976. A Caledonian plate tectonic model. *Journal of the Geological Society,* **132***,* 579–609

PLANK, T., & LANGMUIR, C. H. 1998. The chemical composition of subducting sediment and its consequences for the crust and mantle. *Chemical Geology*, **145**, 325-394.

REED, F. R. C. 1895. The geology of the country around Fishguard. *Quarterly Journal of the Geological Society of London*, **51**, 149–95

ROBINSON, D. & BEVINS, R. E. 1986. Incipient metamorphism in the Lower Palaeozoic marginal basin of Wales. *Journal of Metamorphic Geology*, **4**, 101-103

ROBINSON, D., REVERDATTO, V. V., BEVINS, R. E., POLYANSKY, O. P. & SHEPLEV, V. S. 1999. Thermal modeling of convergent and extensional tectonic settings for the development of low-grade metamorphism in the Welsh Basin. *Journal of Geophysical Research*, **104**, 23,069-23,079

ROLLINSON, H. R. 1993. *Using geochemical data: evaluation, presentation, interpretation* Essex: Longman Scientific & Technical, 352

RUDNICK, R. L. & GAO, S. 2003. Composition of the continental crust. *Treatise on Geochemistry*, **3**, 1-64

SDROLIAS, S. & MÜLLER, R.D. 2006. Controls on Back-arc Basin Formation, *Geochemistry, Geophysics, Geosystems*, **7**, Q04016, doi: 10.1029/2005GC001090

SINTON, J.M., FORD, L., CHAPPELL, B. & MC CULLOCH, M. 2003. Magma genesis and mantle heterogeneity in the Manus back-arc basin, Papua New Guinea. *Journal of Petrology*, **44**, 159–195

STERN, R. J. 2002. Subduction zones. *Reviews of Geophysics*, **40**, 1-13

608 SUN, S. S. & MCDONOUGH, W. 1989. Chemical and isotopic systematics of oceanic
609 basalts: implications for mantle composition and processes. *Geological Society, London,*
610 *Special Publications*, **42**, 313-345
611
612 TATSUMI, Y. & EGGINS, S. 1995. *Subduction Zone Magmatism.* Blackwell, Malden, Mass.
613
614 THOMAS, G. E. & THOMAS, T. M. 1956. The volcanic rocks of the area between Fishguard
615 and Strumble Head, Pembrokeshire. *Quarterly Journal of the Geological Society of*
616 *London*, **112**, 291–314
617
618 THORPE, R. S., LEAT, P. T., MANN, A. C., HOWELLS, M. F., REEDMAN, A. J. & CAMPBELL,
619 S. D. G. 1993. Magmatic evolution of the Ordovician Snowdon volcanic centre, North
620 Wales (UK). *Journal of Petrology*, **34**, 711-741
621
622 TRENCH, A. & T. H. TORSVIK. 1992. The closure of the Iapetus Ocean and Tornquist Sea:
623 new palaeomagnetic constraints. *Journal of the Geological Society,* **149**, 867-87
624
625 VAN STAAL, C. R., WHALEN, J. B., VALVERDE-VAQUERO, P., ZAGOREVSKI, A., &
626 ROGERS, N. 2009. Pre-Carboniferous, episodic accretion-related, orogenesis along the
627 Laurentian margin of the northern Appalachians. *Geological Society, London, Special*
628 *Publications*, **327**, 271-316
629
630 WOOD, D. A., JORON, J. L., & TREUIL, M. 1979. A re-appraisal of the use of trace elements
631 to classify and discriminate between magma series erupted in different tectonic
632 settings. *Earth and Planetary Science Letters*, **45**, 326-336

633 **Figure 1**

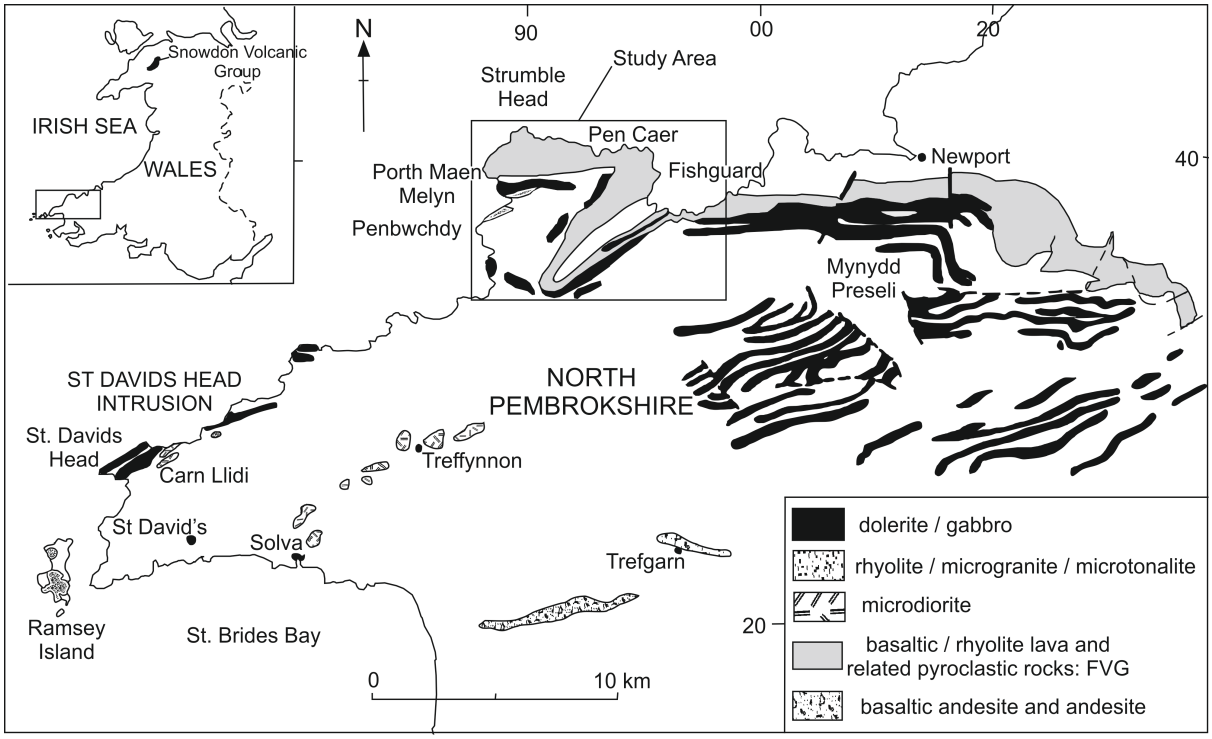

634

635

636 **Figure 2**

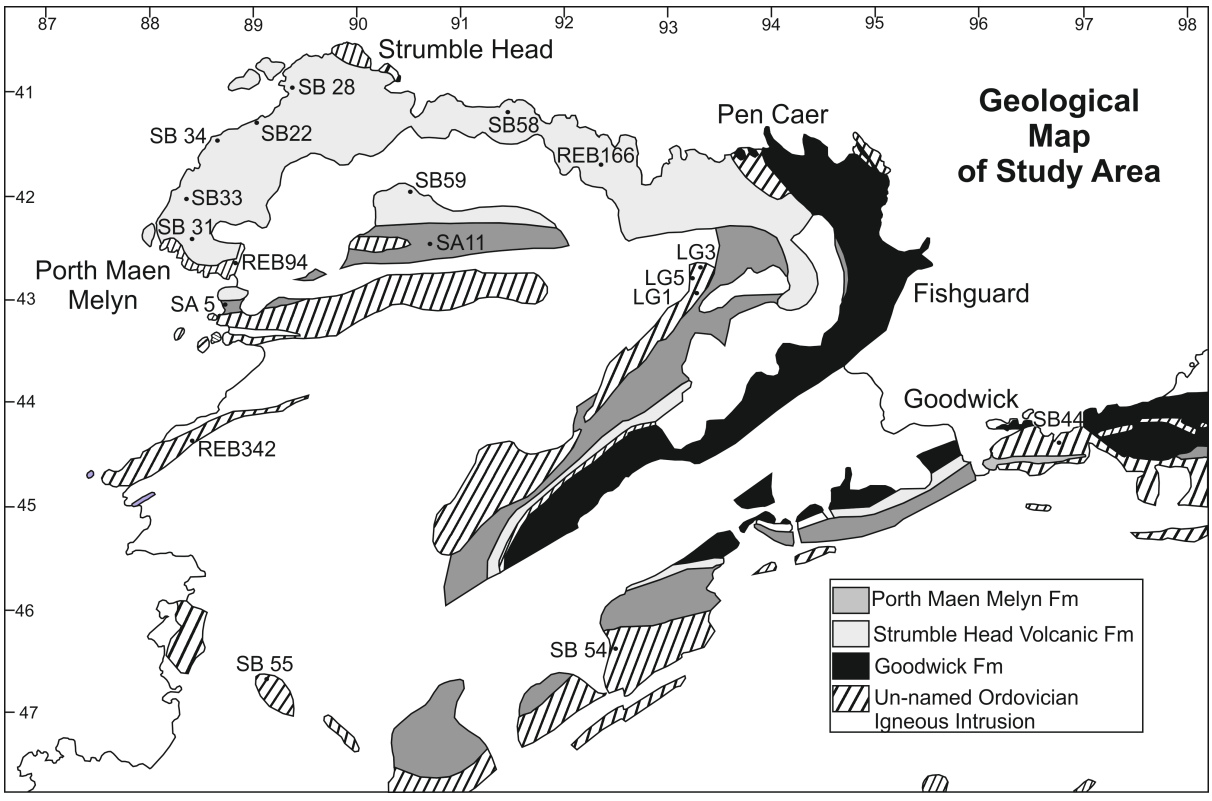

637 **Figure 3**

638

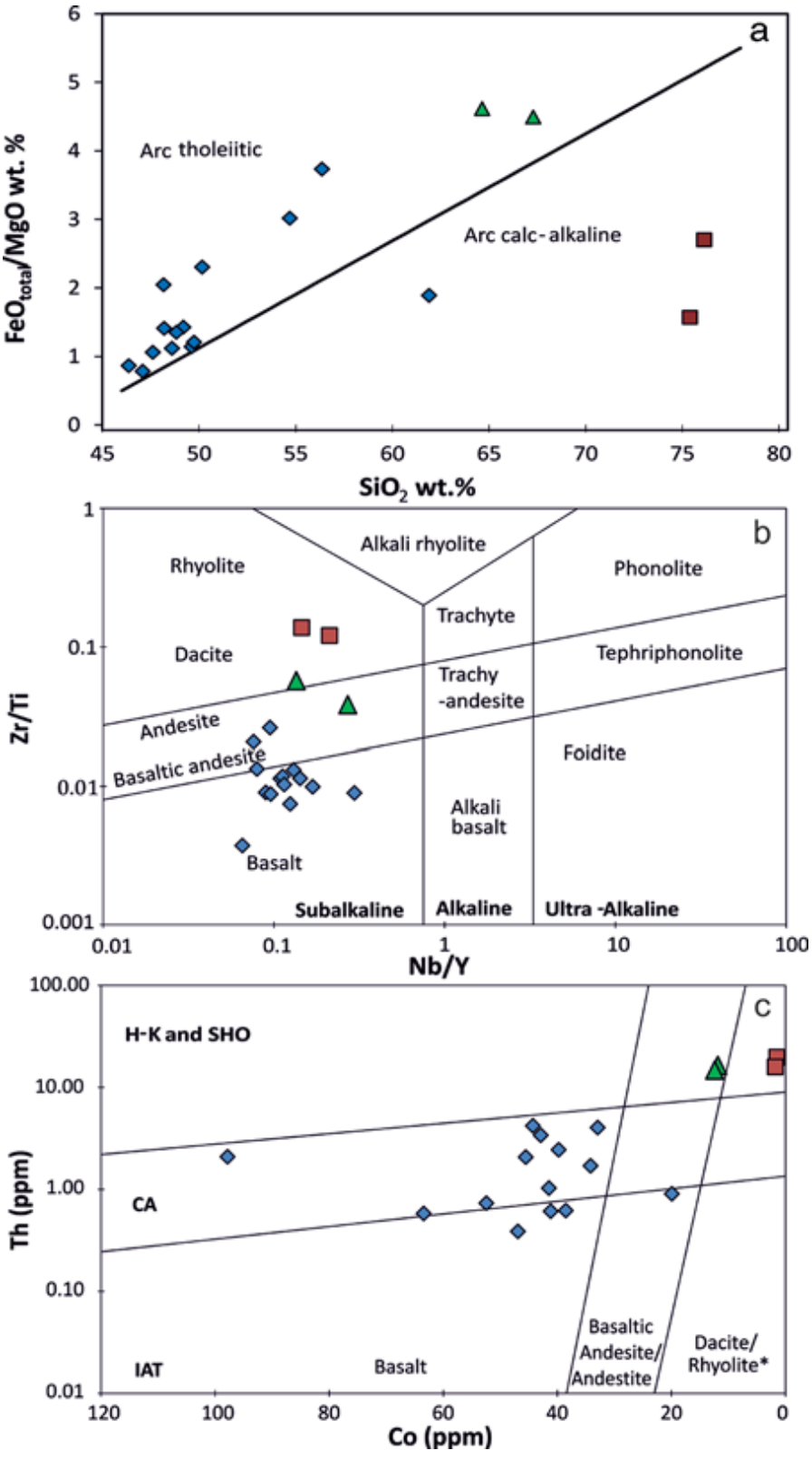

639
640

641 **Figure 4**

642

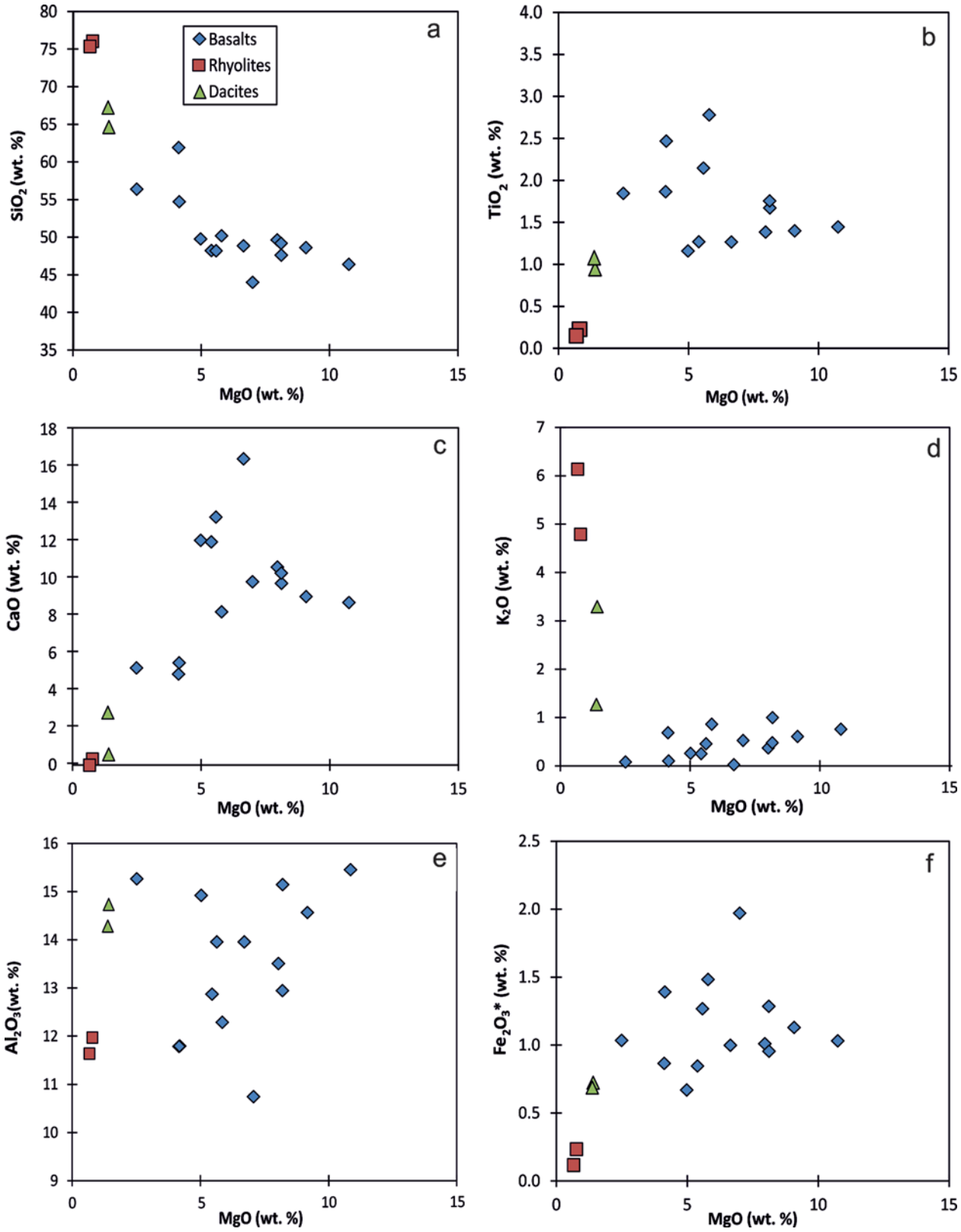

643
644
645

646 **Figure 5**

647

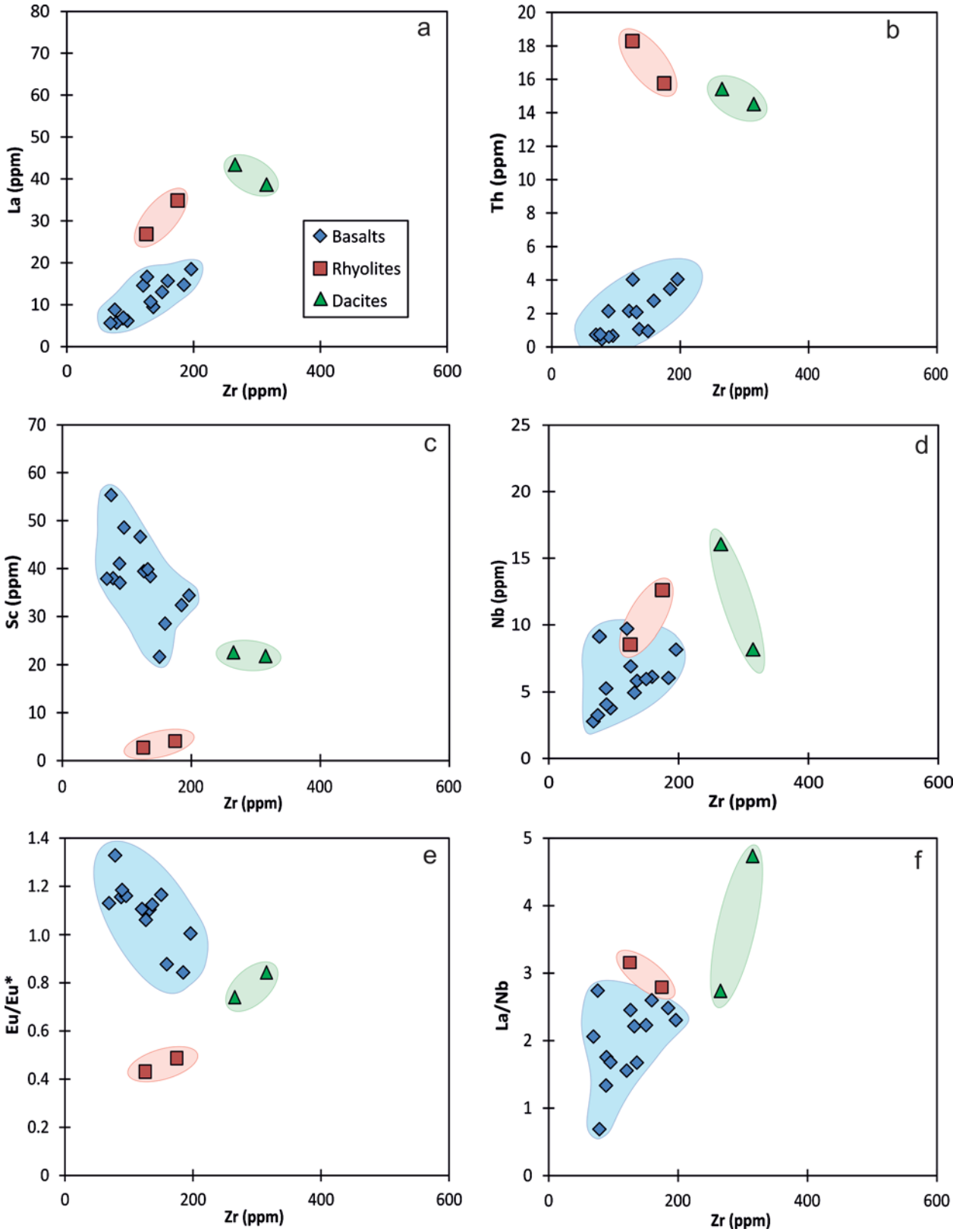

648
649
650

651 **Figure 6**

652

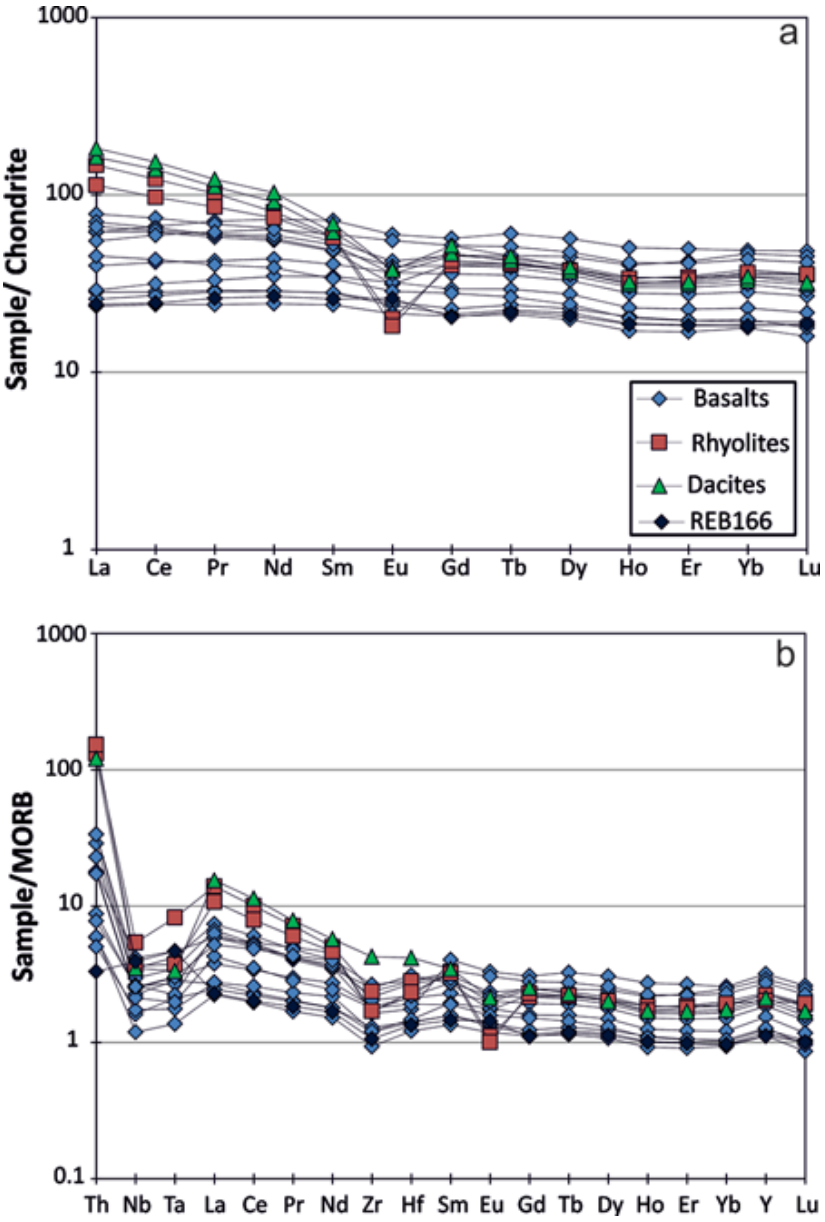

653
654

655

656

657

658

659

660

661 **Figure 7**

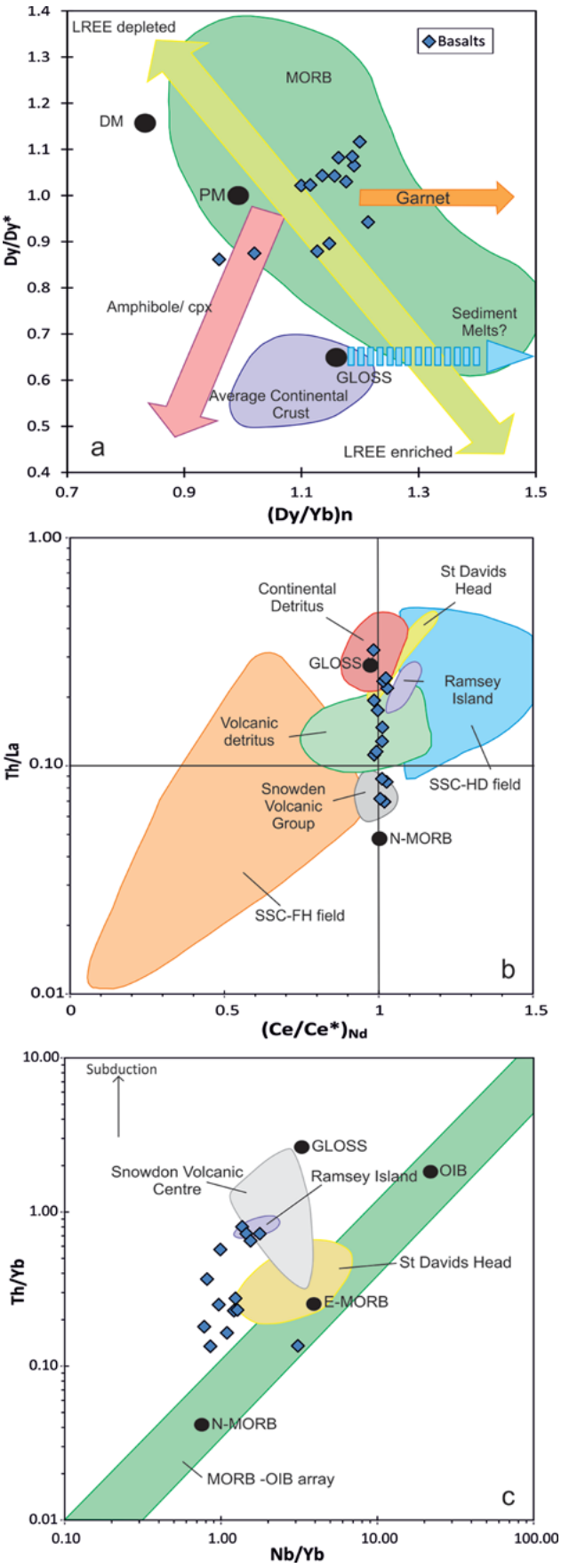

662

663 **Figure 8**

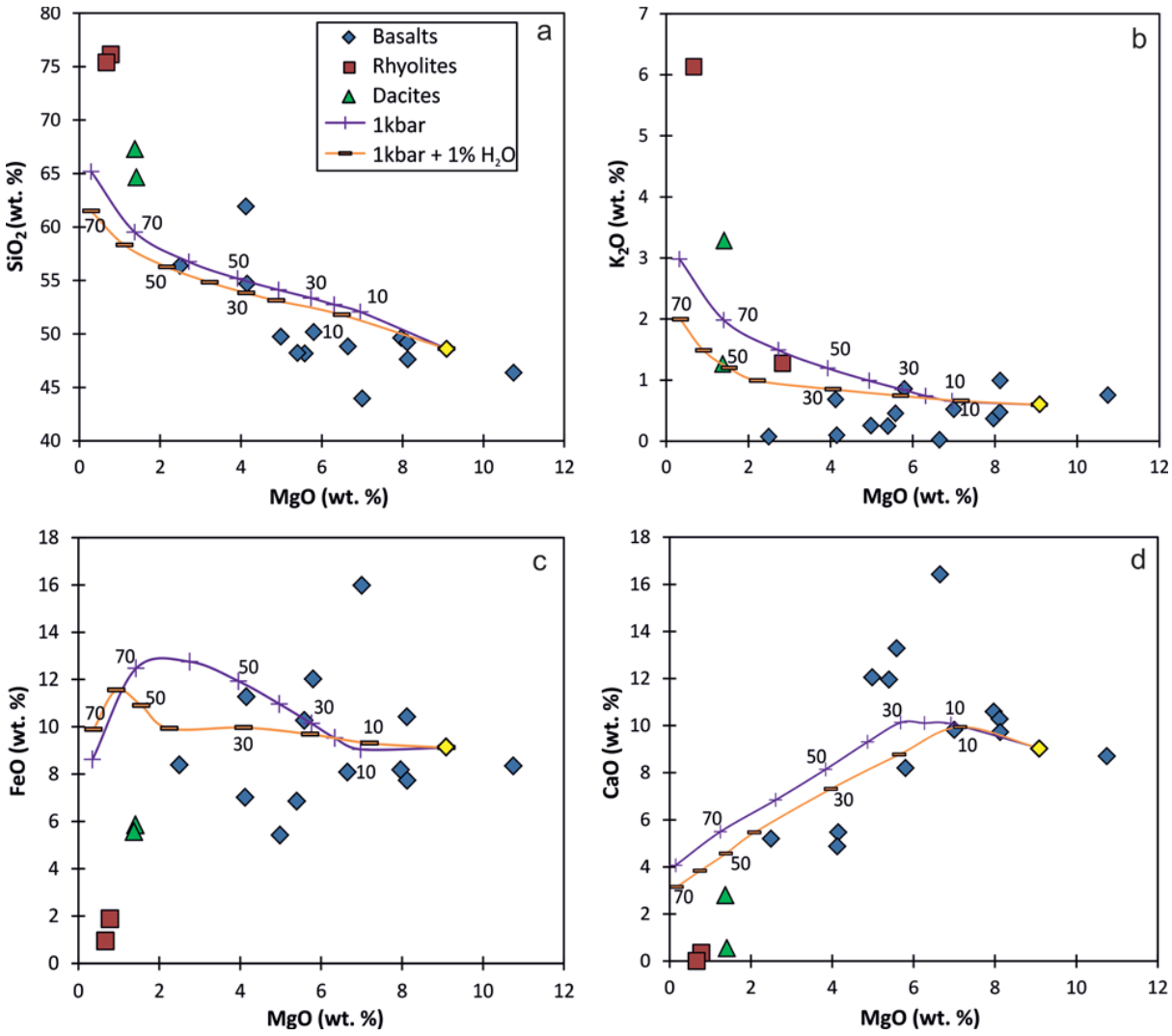

664

665

666

667

668

669

670

671

672 **Figure 9**

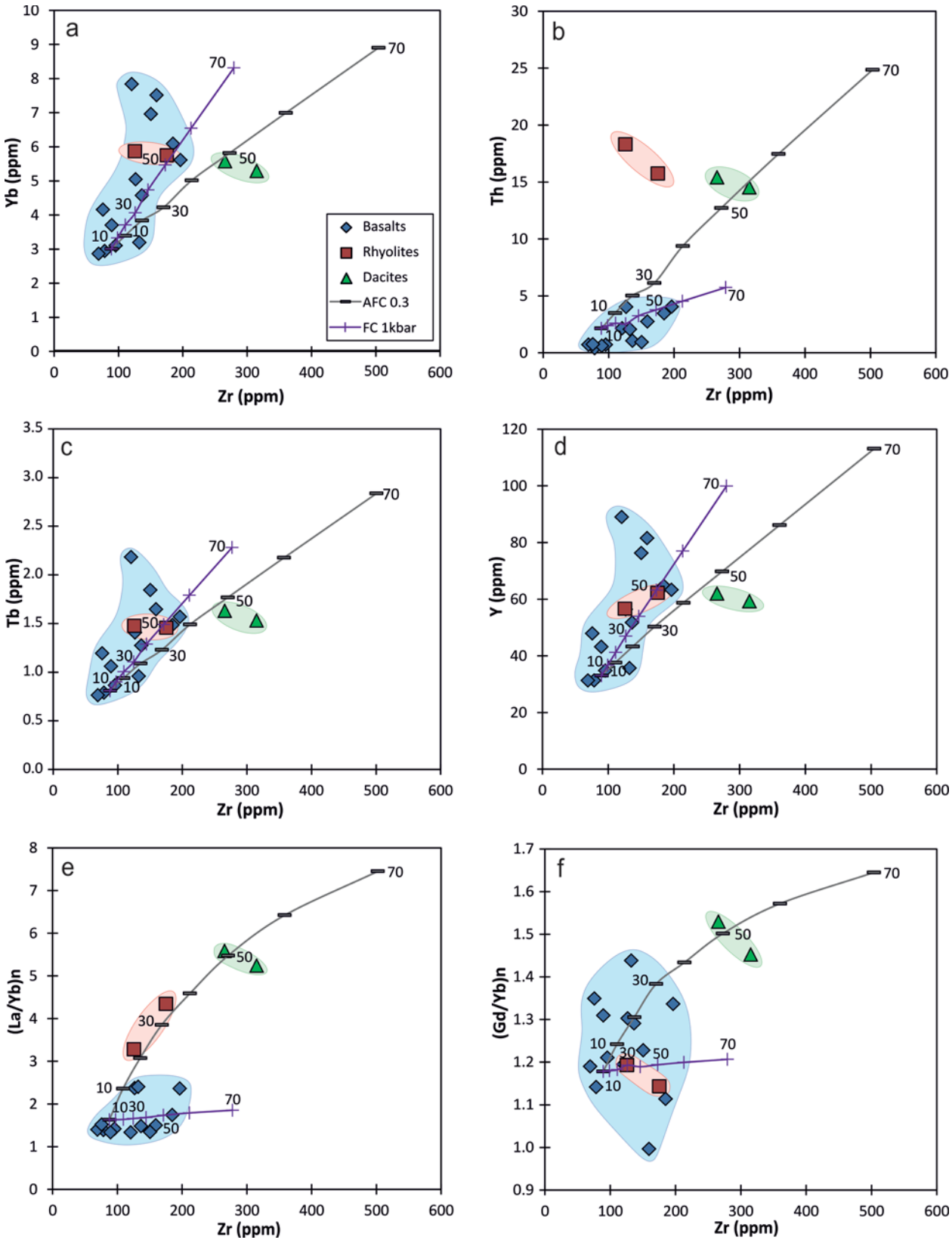

673
674
675

676 **Figure 10**

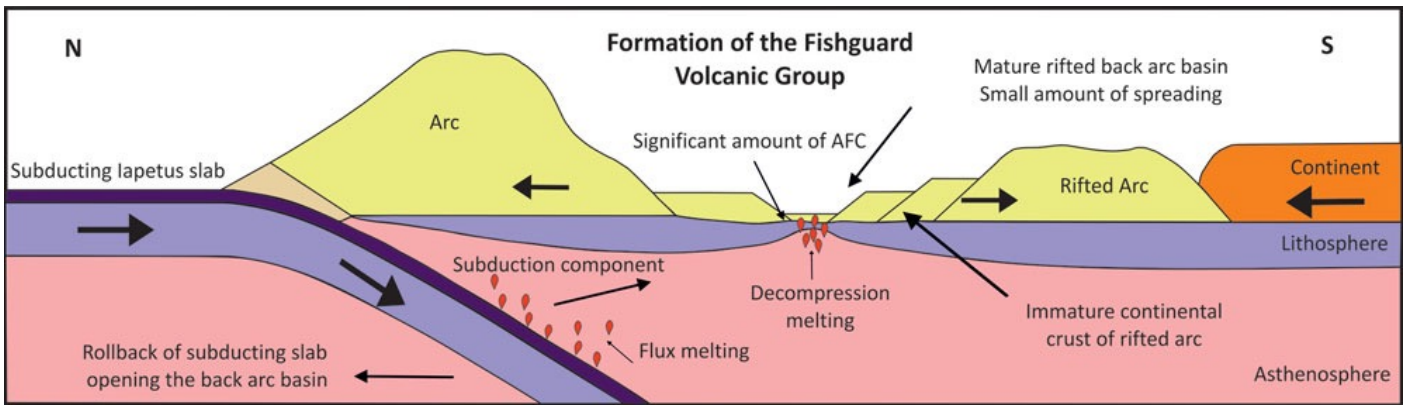

677
678

679 **Figure captions**

680 *Figure 1*. Map adapted from Bevins et al. (1991) showing the location of the Ordovician
681 igneous rocks of North Pembrokeshire and the rest of Wales in relation to one another. The
682 rock types of the study area are also shown.

683

684 *Figure 2*. Geological map showing the locations of the samples analysed in this study. Also
685 highlighted are the formations which have been sampled. The non patterned portion of the
686 map represents unrelated rocks and quaternary cover.

687

688 *Figure 3*. (a) Miyashiro (1975) basalt classification diagram showing the compositions of the
689 studied samples. (b) Nb/Y – Zr/Ti classification diagram adapted from Pearce (2008). (c) Th-
690 Co discrimination diagram (Hastie et al., 2007). The compositional fields are IAT, island arc
691 tholeiite; CA, calc-alkaline; H-K, high-K calc-alkaline; SHO, shoshonite. (*indicates that
692 latites and trachytes also plot in the D/R fields).

693

694 *Figure 4*. Bivariate plots of major element data against MgO (wt.%) for the Fishguard
695 Volcanic rocks.
696
697 *Figure 5*. Bivariate plots of trace elements variation with Zr (ppm) for the Fishguard
698 Volcanic rocks.
699
700 *Figure 6*. (a) Chondrite normalised REE and (b) MORB normalised trace element diagrams
701 (normalising values from Sun & McDonough 1989). Sample REB166, is highlighted.
702
703 *Figure 7.* (a) A Dy/Dy* - Dy/Y plot of Fishguard lavas adapted from Davidson et al. (2013).
704 DM –depleted mantle, PM - primitive mantle (Sun & McDonough, 1989), GLOSS - average
705 global subducting sediment (Plank & Langmuir, 1998). (b) Th/La-$(Ce/Ce^*)_{Nd}$ diagram
706 (Hastie et al. 2013) showing the potential sedimentary slab components that may have
707 contaminated the source region. SSC- HD - slow sediment clay-hydrogenous, SSC-FH - slow
708 sediment clay-fish debris/ hydrothermal. (c) The Th/Yb-Nb/Yb diagram from Pearce (2008).
709 An enrichment in Th relative to the equally-incompatible Nb acts as an effective proxy of
710 subduction input. Representative fields for other Welsh lower Ordovician volcanic complexes
711 are also plotted on (b) and (c) for comparison. The data for Ramsey Island and St Davids
712 Head were obtained from Bevins et al. (1991) and the Snowdon data from Thorpe et al.
713 (1993).
714
715 *Figure 8*. Bivariate diagrams of selected major elements vs. MgO for the Fishguard
716 volcanics along with modelled fractional crystallisation trends (1kb anhydrous and 1kb with
717 1% H_2O added) for a parental magma with a composition of sample LG3. Markers on the
718 modelled trends are at intervals of 10% crystallisation.

719

720 *Figure 9*. Bivariate diagrams for representative trace elements and incompatible trace element
721 ratios showing the results for AFC and fractional crystallisation, where 0.3 AFC is equal to
722 30% additional contamination and represents the model which best replicates the
723 geochemical trend of the Fishguard Volcanic Group.

724

725 *Figure 10*. Proposed model for the formation of the Fishguard Volcanic Group. The diagram
726 shows the tectonic configuration of the Iapetus slab subducting below the Avalonia continent,
727 with rollback of the subducting slab facilitating the rifting of the arc and opening of the back-
728 arc basin. This rifting leads decompression melting in the structurally weaker parts of the
729 basin; these magmas mix with melts associated with fluids from the subducting sediments. A
730 small amount of crustal contamination occurs as the melts rise through the rifted arc crust.

731

732

733

734

735

736

737

738

739

740

741

742

743

744 **Table 1** Major and trace element data for the Fishguard Volcanic Group

Sample:	LG3	LG1	LG5	REB166	SB22	SB59	SB54	SB34	SB28
Major elements (wt.%)									
SiO_2	48.61	49.63	49.19	46.37	48.17	49.74	54.7	48.83	47.61
TiO_2	1.40	1.38	1.75	1.44	2.14	1.16	2.47	1.26	1.67
Al_2O_3	14.57	13.5	12.94	15.45	13.95	14.92	11.79	13.96	15.15
MnO	0.20	0.18	0.23	0.17	0.19	0.17	0.24	0.15	0.16
MgO	9.09	7.97	8.12	10.75	5.58	4.98	4.15	6.65	8.13
CaO	9.03	10.60	10.28	8.70	13.29	12.04	5.47	16.42	9.73
Na_2O	3.55	3.52	2.81	2.35	2.12	3.69	4.41	0.66	3.46
K_2O	0.60	0.37	0.47	0.75	0.45	0.25	0.10	0.02	0.99
P_2O_5	0.13	0.14	0.19	0.13	0.29	0.17	0.31	0.13	0.21
FeO*	10.17	9.09	11.58	9.28	11.42	6.02	12.52	8.99	8.60
LOI	2.55	2.52	2.16	3.94	2.09	7.00	2.18	3.38	3.80
Total	99.90	98.90	99.72	99.33	99.69	100.14	98.34	100.45	99.51
Trace elements (ppm)									
Be	0.6	0.6	1.7	0.7	1	1	1.7	0.6	0.6
Sc	42	50	48	39	39	33	35	39	38
V	265	278	338	256	354	183	336	251	306
Cr	273	67	91	361	106	132	6	322	333
Co	46	41	98	47	42	43	35	39	64
Ni	24	18	13	52	23	49	16	29	87
Cu	126	105	106	79	84	87	82	133	70
Zn	55	19	49	47	46	32	81	23	64
Ga	18.8	19.2	44	21.4	25.4	25.4	24.5	26.6	23
Rb	13.3	6.8	22.2	10.2	5.8	4.5	1.8	0.2	20.7
Sr	244	293	200	259	490	85	106	363	239
Y	33	34.8	89	31.3	51.7	64.6	63.3	31.3	43.2
Zr	88.6	95.6	120.8	78.6	136.5	184.8	196.4	69.2	89.5
Nb	5.25	3.76	9.70	9.14	5.82	6.04	8.17	2.77	4.04
Mo	0.32	0.14	0.59	0.14	1.72	0.10	0.13	0.41	0.25
Sn	1.88	1.62	2.64	1.83	0.52	0.67	0.82	0.44	0.54
Cs	1.56	0.85	0.88	1.39	0.46	0.34	2.22	0.30	1.07
Ba	114	81	157	134	160	71	226	7	52
La	6.72	6.12	14.60	5.71	9.44	14.76	18.47	5.59	6.89
Ce	17.38	16.60	40.66	15.07	25.56	37.72	45.39	14.77	19.35
Pr	2.69	2.64	6.59	2.42	3.94	5.35	6.35	2.23	3.06
Nd	13.15	13.10	33.25	12.23	19.95	25.30	29.58	11.12	15.88
Sm	4.14	4.15	10.62	3.83	6.02	7.13	8.11	3.55	5.12
Eu	1.34	1.40	3.37	1.47	2.05	1.77	2.38	1.21	1.81
Gd	4.22	4.54	11.32	4.06	7.14	8.20	9.06	4.12	5.86
Tb	0.81	0.86	2.18	0.79	1.27	1.49	1.57	0.76	1.06
Dy	5.33	5.62	13.93	5.11	8.08	9.49	9.84	4.88	6.79
Ho	1.03	1.13	2.75	1.02	1.52	1.84	1.87	0.93	1.26

Er	2.96	3.14	7.94	2.93	4.41	5.56	5.42	2.70	3.62
Tm	0.46	0.49	1.21	0.45	0.73	0.93	0.88	0.45	0.59
Yb	2.96	3.10	7.84	2.95	4.57	6.09	5.61	2.87	3.70
Lu	0.46	0.47	1.19	0.46	0.66	0.88	0.82	0.39	0.53
Hf	2.88	2.91	3.61	2.75	4.35	6.38	5.83	2.49	3.02
Ta	0.38	0.28	0.62	0.62	0.40	0.36	0.56	0.18	0.23
Th	2.14	0.71	2.15	0.40	1.05	3.46	4.04	0.72	0.60
U	0.31	0.28	0.62	0.17	0.34	0.94	1.07	0.27	1.10
Sample:	SB31	SB58	SB33	SB55	SB44	SA5	SA11	REB342	REB94
Major elements (wt.%)									
SiO_2	50.16	48.2	61.9	56.37	43.95	76.13	75.4	64.65	67.29
TiO_2	2.78	1.27	1.86	1.84	3.54	0.23	0.15	0.95	1.08
Al_2O_3	12.29	12.87	11.79	15.26	10.74	12	11.64	14.73	14.28
MnO	0.22	0.15	0.16	0.21	0.28	0.04	0.02	0.16	0.15
MgO	5.8	5.4	4.12	2.5	7	0.78	0.67	1.41	1.38
CaO	8.2	11.95	4.87	5.19	9.82	0.35	0.003	0.55	2.8
Na_2O	3.3	4.24	4.41	6.76	2.26	3.44	2.18	3.55	3.48
K_2O	0.86	0.25	0.68	0.07	0.52	4.79	6.13	3.28	1.26
P_2O_5	0.29	0.32	0.21	0.52	0.4	0.05	0.01	0.24	0.26
FeO*	13.36	7.61	7.8	9.32	17.75	2.1	1.05	6.51	6.19
LOI	2.02	7.96	1.69	1.41	2.35	0.74	0.66	2.39	1.93
Total	99.28	100.22	99.49	99.45	98.61	100.65	97.91	98.42	100.1
Trace elements (ppm)									
Be	1.3	1.3	1.2	1.3	0.9	2.1	2.1	2.8	2.9
Sc	41	29	41	22	57	4	3	22	23
V	440	179	325	98	854	10	1	96	129
Cr	19	122	100	10	48	24	11	23	29
Co	44	40	36	20	53	1	1	12	11
Ni	5	27	15	2	50	2	4	3	3
Cu	40	64	20	40	100	31	12	34	39
Zn	66	37	51	43	59	56	16	23	45
Ga	23.1	23.6	17.7	26.9	24.5	19.5	19.3	26.8	27.3
Rb	15.3	3.7	10.9	1.3	7.9	84.4	182.2	105.1	55.0
Sr	200	133	163	242	193	56	38	101	303
Y	56.4	81.5	35.7	76.3	47.9	62.3	56.6	59.2	62.0
Zr	127	160	132	151	76	175	126	315	266
Nb	6.90	6.12	4.94	5.96	3.25	12.59	8.55	8.17	16.05
Mo	0.32	1.46	0.14	0.24	0.26	1.61	0.64	0.51	0.66
Sn	0.60	0.72	0.63	0.57	0.50	3.40	0.73	0.54	0.98
Cs	0.61	0.92	0.50	0.64	0.83	0.82	0.91	2.25	1.89
Ba	278	171	191	45	147	752	493	931	594
La	16.65	15.68	10.71	13.02	8.79	34.85	26.87	38.65	43.38
Ce	40.01	38.52	26.49	36.32	23.74	75.13	59.46	85.33	93.95
Pr	5.55	5.54	3.74	5.72	3.66	9.45	7.94	10.34	11.37
Nd	25.96	27.07	17.76	29.20	19.22	36.66	33.95	41.80	47.02

Sm	7.23	7.77	4.98	8.86	5.87	8.65	8.48	9.10	10.18
Eu	2.23	2.02	1.61	3.11	1.99	1.13	1.02	2.17	2.12
Gd	7.94	9.05	5.56	10.33	6.78	7.95	8.47	9.29	10.31
Tb	1.41	1.65	0.96	1.84	1.19	1.46	1.48	1.53	1.63
Dy	8.69	11.01	5.93	11.70	7.56	9.27	9.18	9.11	9.63
Ho	1.65	2.19	1.10	2.26	1.43	1.85	1.73	1.71	1.76
Er	4.81	6.76	3.12	6.59	4.13	5.50	5.29	5.02	5.16
Tm	0.77	1.16	0.50	1.08	0.66	0.90	0.93	0.80	0.85
Yb	5.04	7.51	3.20	6.96	4.16	5.75	5.87	5.29	5.57
Lu	0.71	1.11	0.44	1.02	0.60	0.87	0.88	0.77	0.79
Hf	4.47	5.55	3.93	4.50	2.43	5.77	4.79	8.57	7.91
Ta	0.46	0.30	0.26	0.40	0.21	1.09	0.49	0.44	0.88
Pb	6.76	7.22	5.34	2.45	7.34	18.68	21.89	19.23	24.86
Th	4.03	2.75	2.07	0.93	0.75	15.75	18.31	14.52	15.42
U	1.04	1.34	0.68	0.31	0.22	4.01	4.54	3.40	3.77

* denotes total iron